JOURNAL OF THERMOPHYSICS AND HEAT TRANSFER
Vol. 21, No. 3, July–September 2007

Laser-Induced Fluorescence Measurements of Atomic Oxygen Using Two Calibration Methods

Stefan Löhle* and Monika Auweter-Kurtz†
University of Stuttgart, 70569 Stuttgart, Germany

DOI: 10.2514/1.26902

Number densities of atomic oxygen have been measured in pure oxygen plasma, using two-photon laser-induced fluorescence measurements. In this paper, two calibration techniques are compared: the sensitivity of the experimental setup is calibrated using scattering experiments, and reference measurements on xenon are performed using two-photon laser-induced fluorescence measurements. The theoretical background and the experimental setup are described in detail. The advantages and drawbacks are herewith outlined. Applied to high-enthalpy, pure oxygen plasma, the evaluated number densities show fairly good agreement; however, because a constant discrepancy is measured between the results when using the two calibration approaches, a systematic error is probable. Possible reasons for this error are discussed (e.g., the cross-sectional ratio, in the case of xenon reference measurement calibration). One main conclusion is that measurements that are performed using the reference measurements on xenon are preferred, because they have much fewer experimental factors to be taken into account.

Nomenclature

A_L	=	laser beam area, m^2
A_{21}	=	Einstein coefficient, s^{-1}
E_L	=	laser energy, J
e	=	electron charge 1.6022×10^{-19} C
$F(t)$	=	temporal function of the laser pulse, s
G_a/C	=	preamplifier gain/capacitance ratio
G_{PMT}	=	photomultiplier amplification
$G^{(2)}$	=	correlation factor of the laser field
$\dot{m}$	=	mass flow, g/s
n_b	=	refraction
p_a	=	ambient pressure, Pa
QE	=	quantum efficiency of the photomultiplier
Q_{21}	=	quenching rate, s^{-1}
S	=	fluorescence, J
s	=	reference condition
sens	=	sensitivity of the boxcar
U_A	=	anode voltage, V
V_R	=	Rayleigh signal, V
η	=	optical efficiency
λ	=	wavelength, nm
ν	=	wavelength, s^{-1}
$\sigma_\omega^{(2)}$	=	absorption cross section, m^4s
τ_p	=	pulse time, s
τ_{LT}	=	effective lifetime, s
ω	=	transition frequency, s^{-1}
$(\mathrm{d}\sigma/\mathrm{d}\Omega)_{\mathrm{pol}}^{90\,\mathrm{deg}}$	=	Rayleigh cross section, m^2
$\hbar$	=	Planck constant divided by 2π, 1.055×10^{-34} Js

I. Introduction

THERMAL protection systems for Earth reentry maneuvers are currently qualified using plasma wind-tunnel facilities [1,2] in which the high-enthalpy air plasma flows that are expected for the reentry mission to be investigated are generated. To make progress in the development of future thermal protection systems (e.g., reusable systems), the chemical behavior of candidate materials has to be understood in more detail. A simplification of the chemical processes by using only pure gas flows (i.e., pure nitrogen and pure oxygen high-enthalpy plasma flows) can be seen as a first step and is particularly helpful to validate physical models and to investigate the catalytic and oxidation behavior of the material [2]. High-enthalpy pure nitrogen flows can easily be generated using arc-jet generators, and the material behavior has been investigated thoroughly [3]. Pure oxygen plasma flows, however, are more difficult to generate, because the high dissociation degree of the oxygen molecule leads to rapid erosion processes of any electrode material. Hence, electrodeless inductively heated plasma generators are the only experimental facilities to perform steady-state basic thermal protection material experiments using pure oxygen as the driver gas. This advantage of high-enthalpy plasma generation without any electrode is also beneficial for entry simulation into atmospheres with a significant amount of CO_2, such as Mars or Venus [4,5].

The experiments described here are designed to add particular details to the existing knowledge of high-enthalpy pure oxygen plasmas. This, in turn, can be used for testing and refining computational models and planned flight experiments [6]. The experiments are aimed at detecting the most important constituent of the pure oxygen plasma in terms of chemical behavior: atomic oxygen. The number densities are measured by detecting the two-photon absorption laser-induced fluorescence (LIF). First results were presented by the authors in 2005 [7]. The physical principle of LIF measurements is sketched in Fig. 1. Oxygen atoms in ground electronic state are excited via the $3p^3P_{2,1,0} \leftarrow 2p^3P_2$ two-photon transition at about 226 nm. The two-photon process is chosen, because a single-photon absorption process would require a vacuum ultraviolet absorption, due to the large energy difference between the ground state and the excited states. This, in turn, requires a very complex experimental setup that is difficult to apply to large facilities, such as plasma wind tunnels [8]. The following fluorescence is measured using the $3p^3P_{2,1,0} \rightarrow 3s^3S_1^0$ transition at 844.5 nm. The excitation is performed using a pulsed laser system and the fluorescence is detected using a photomultiplier, a fast oscilloscope, and gated integrators. The measurement setup and equipment is described in detail in the following paragraph.

The main problem of the measurement technique is the calibration procedure of the measurement signals. Known approaches are based on titration experiments and actinometry [9]. The present paper deals with a comparison of measured results using an almost-standard

Presented as Paper 3444 at the 25th AIAA Aerodynamic Measurement Technology and Ground Testing Conference, San Francisco, CA, 5–8 June 2006; received 31 July 2006; revision received 18 October 2006; accepted for publication 18 October 2006.

*Research Engineer, Institut für Raumfahrtsysteme, Pfaffenwaldring 31.
†Professor, Institut für Raumfahrtsysteme, Pfaffenwaldring 31. Associate Fellow AIAA.

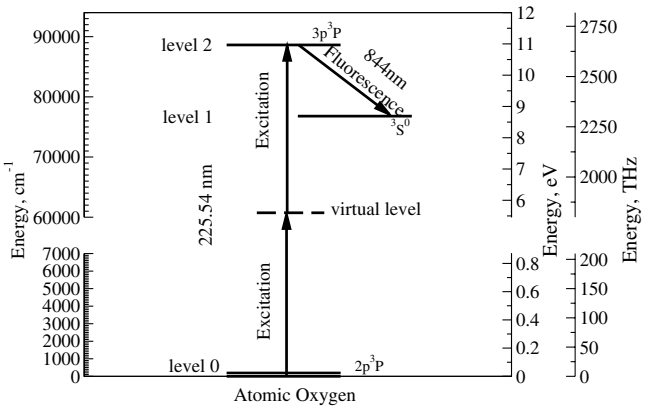

Fig. 1 Energy-level diagram for atomic oxygen.

approach first published by Bamford et al. [10] and a recently published approach by the working group of Döbele [10–12] that has been adapted for use in the plasma wind-tunnel facility at the Institut für Raumfahrtsysteme (IRS). The standard technique follows the strategy of calibrating the experimental setup, using light scattering experiments for absolute calibration of the number density. The new approach, however, uses comparative measurements of a two-photon absorption LIF of a nearby rare gas at known density. This is xenon, in the case of atomic oxygen. The approach using comparative measurements has already been applied by Grinstead et al. [13] at Nasa Ames to quantify atomic nitrogen. The authors conclude that the measurement error can be significantly reduced using this approach, although they do not provide absolute number density measurements. In this paper, both calibration procedures are described, the advantages and the drawbacks are outlined, and the measurement errors are quantified and discussed.

In the following paragraph, the experimental setup is described. Then, both theoretical approaches are briefly described; the main emphasis lies on the alternative approach using xenon measurements, because the standard approach is relatively well known. Results and their interpretation are presented in the next section, followed by a conclusion summarizing the main output of this work.

II. Experimental Setup

The facility used for the present investigation is called Plasmawindkanal 3 (PWK3). A schematic of the setup is shown in Fig. 2. It consists of a vacuum vessel 2 m in diameter and 2.5 m in length. Optical accesses on both sides of the vacuum chamber are provided in order to measure and observe the plasma flow. The plasma generator depicted in a sectional view in Fig. 3 is installed in the front lid. On the rear end, the vacuum chamber is connected to the IRS's vacuum system [14].

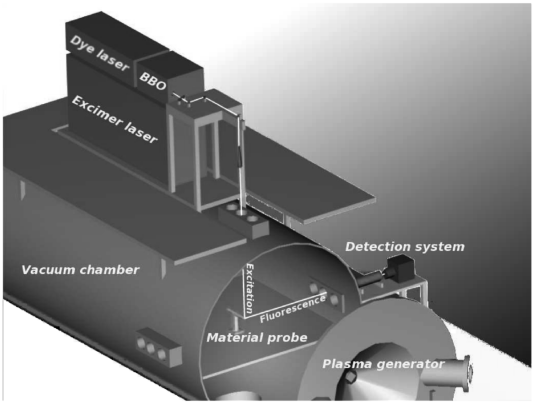

Fig. 2 Schematic of the experimental setup at PWK3.

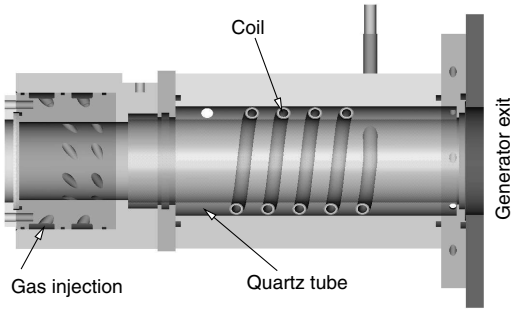

Fig. 3 Inductive plasma generator IPG3.

The plasma is generated inside a thin quartz tube by a high-frequency current applied to the induction coil around the tube. The coil has 5.5 turns. Together with four capacitors, the coil builds a resonant circuit at a frequency of 640 kHz that is switched to the power supply. The maximum electrical power is 375 kW. The water cooling system surrounds both the quartz tube and the induction coil. The working fluid is fed into the quartz tube on one side using a tangential injection. The alternating current in the coil induces an electric field in the tube and this electric field initiates an electric discharge in the gas. The produced plasma finally expands into the vacuum chamber [5]. The adjustable parameters are mass flow rate, ambient pressure in the vacuum chamber, and anode voltage of the power supplying triode. In the present case, all measurements have been performed at minimum ambient pressure, which is $p_a = 26$ Pa. The measurement condition also depends on the distance of the measurement location with respect to the generator exit. Because of constraints of optical access to the vacuum chamber, all measurements had to be performed at a distance of 140 mm.

The application of the experimental setup for laser spectroscopy at PWK3 is also shown in Fig. 2. The laser system is installed on top of the vacuum chamber. It consists of a pulsed excimer gas laser used with XeCl emitting at 308 nm (Lambda Physik CompEX 205). With a dye laser (Lambda Physik Scanmate 2E) and a beta barium borate (BBO) crystal for frequency-doubling, laser radiation at 225 nm is attained with a maximum output of about 1 mJ per pulse. The laser line width at 225 nm is $\Delta\lambda = 0.000567$ nm. The laser beam is adjusted to the measurement location on the plasma jet axis in the center of the vacuum chamber by three prisms and a focusing lens system.

Laser-induced fluorescence is detected at right angles to the laser and the flow direction. A gated photomultiplier tube (PMT) is used (Hamamatsu R636-10). Two achromatic lenses image the fluorescence plane onto the detector. In front of the entrance slit, an interference filter is installed that transmits light at the wavelength of interest and blocks light at other wavelengths. For the measurements of atomic oxygen, a filter (L.O.T-Oriel 850FS20-50) has been used, and for the measurements of xenon, a 460FS10-50 has been mounted. The transmission at the wavelengths of interest is $\eta_{\mathrm{Xe}} = 0.42$ for the xenon measurement and $\eta_{\mathrm{O}} = 0.62$ in the case of atomic oxygen.

The data acquisition equipment consists of two boxcar integrator channels (Stanford Research Systems SR250) and a computer interface (Stanford Research Systems SR245). Data acquisition is controlled by a LabView program and a trigger generator (Stanford Research Systems DG535) in order to switch the photomultiplier gate with respect to the laser pulse. Laser energy measurement is performed with an energy monitor (Polytec RjP735). A beam splitter is used that splits a small amount of laser energy to the energy monitor. Measurements before the LIF experiments showed that in the needed wavelength range, the amount of laser energy that is split is independent of the incoming laser energy [15]. The measurements are concurrently observed by a fast 1-GHz oscilloscope (Gagescope 82G) in order to evaluate effective lifetimes of the upper state. It is integrated in the data acquisition computer such that the whole experiment is controlled by only one LabView program in which each laser pulse, as well as each time-resolved signal, is visualized during experiments and stored for later data analysis.

III. Theory

The main problem of quantitative laser-induced fluorescence measurements is always how to calibrate the applied experimental setup. There are, classically, two possible approaches. On one hand, the sensitivity of the detector can be calibrated, that is, a measurement is performed in order to connect the measured signal at the data acquisition (usually in volts) to the number of photons that are emitted by the atoms of interest. On the other hand, the relative measurement signals can be quantified if a known number density of the atom of interest is generated and measured using the applied experimental setup. The second approach is particularly difficult in the case of atomic oxygen, because the generation of a precisely known amount of atomic oxygen is already a challenging task. The classically applied approach for high-enthalpy plasma flows follows the first possibility, that is, to calibrate the sensitivity of the experimental setup. Here, scattering experiments are usually applied [10]. The scattering of laser light as a function of wavelength and laser energy is well known, and the wavelength and the laser energy can be thoroughly measured. The main problem of this procedure is that it has to be assumed that the generated scattered light corresponds to the fluorescence signal in terms of optical and geometrical parameters.

A very new approach is to calibrate the experimental setup by reference measurements with a noble gas of known concentration. In the case of atomic oxygen measurements, xenon can be used as reference gas because it fulfills the prerequisites that it can be excited with the same spatial, temporal, and, especially, spectral intensity distribution as atomic oxygen. In fact, the intensity distribution is not even needed if the identical experimental setup is used and the two-photon resonances are very close.

In general, the measured two-photon fluorescence signal can be estimated using simple rate equations, taking into account the energy levels as depicted in Fig. 1. The two-photon absorption is modeled by a quadratic laser photon flux together with a so-called two-photon absorption cross section. For unsaturated two-photon excitation, the fluorescence signal can finally be written as

$$S = \frac{\Omega}{4\pi} V_c \eta \frac{1}{\hbar\omega_{02}} \frac{A_{21}}{A_{21}+Q_{21}} \frac{E_L^2}{A_L^2} \int F^2(t)\,\mathrm{d}t \sigma_\omega^{(2)} n_0 \qquad (1)$$

where Ω is the observed solid angle and V_c is the observed fluorescence collecting volume [10,15]. The absorption coefficient $\sigma_\omega^{(2)} = G^{(2)}\hat{\sigma}_\omega^{(2)}$, where the factor $G^{(2)}$ is accounting for fast fluctuations of the laser pulse, is taken from Bamford et al. [10] ($G^{(2)}\hat{\sigma}_\omega^{(2)} = 4.85 \times 10^{-54}$ m^{4}s). For the dye-laser system in use, $G^{(2)} = 2$, because of the chaotic characteristic of the field. The temporal profile of the laser was measured before the LIF experiments, using a fast-responding photodiode (Thorlabs DET200) with a rise time of 1 ns. It can be assumed that the temporal profile is constant, which has been shown by analyzing more than 100 laser pulses [15]. Figure 4 shows two pulses together

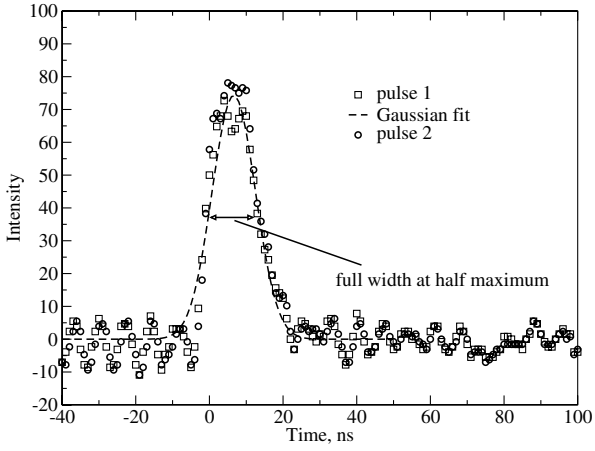

Fig. 4 Temporal profile of the laser pulse.

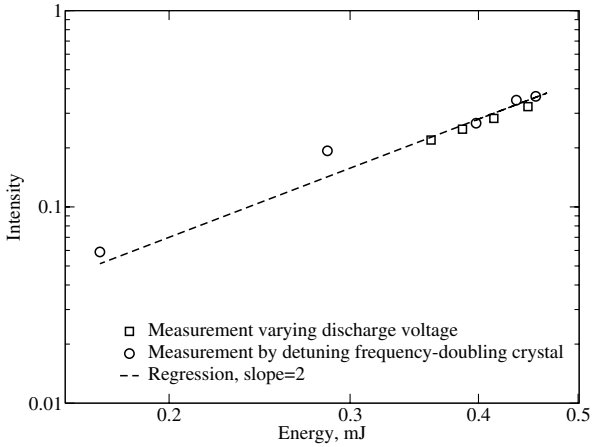

Fig. 5 Quadratic dependence of the fluorescence on the laser energy for atomic oxygen measurement (logarithmic scale).

with a Gaussian fit. From its full width at half maximum, a laser pulse duration of $\tau_p = 13.85 \pm 1$ ns is estimated. The integral of the square of the profile is then

$$\int F^2(t)\,\mathrm{d}t = \frac{1}{\sqrt{\pi}\tau_p} \qquad (2)$$

Before the experiments, the quadratic dependency of the fluorescence on the laser energy was checked to assure that the measurements are performed in a linear regime [see Eq. (1)]. The energy is varied by turning the frequency-doubling crystal while holding the wavelength on the maximum absorption frequency. Figure 5 shows that the quadratic dependency is given. To assure that the dependency does not come from perturbations due to the frequency-doubling process and that the characteristic properties of the laser beam with respect to spatial mode and intensity distribution are not influenced, a variation of the laser energy by varying the discharge voltage of the excimer laser has been additionally performed, leading to the same result (see the squares in Fig. 5).

The fluorescence quantum yield $A_{21}/(A_{21}+Q_{21})$ accounts for fluorescence signal losses due to nonradiating deexcitation (e.g., by collisions). All nonradiating processes are summed up in the quenching rate. In the present case, the fluorescence is measured time-resolved using the oscilloscope. The fluorescence lifetime τ_{LT} is derived from the exponential decay of the fluorescence signal and corresponds to the fluorescence quantum yield, in the form

$$\frac{A_{21}}{A_{21}+Q_{21}} = A_{21}\tau_{\mathrm{LT}} \qquad (3)$$

The Einstein coefficient of spontaneous emission for atomic oxygen is taken from [16] as $A_{21} = 2.89 \times 10^7$ s^{-1}. Figure 6 shows an exemplary result of the fluorescence decay and an exponential fit.

A. Calibration Using Scattering Experiments

As previously mentioned, the recorded signal can be related to the number density of the investigated atoms if the sensitivity of the experimental setup is measured (e.g., by a calibration measurement). Bamford et al. [10] used Raman scattering experiments, but in the present case, Rayleigh scattering experiments are applied to relate the measured signal by a calibration constant D to the number of emitted photons. The Raman scattering signal is too weak for the measurements in PWK3 at IRS [17]. The calibration constant is as follows:

$$D = \eta L_c \frac{\Omega}{4\pi} G_{\mathrm{PMT}} G_a / C e K_s Q E \qquad (4)$$

From Eq. (1) together with Eq. (4), the number density becomes

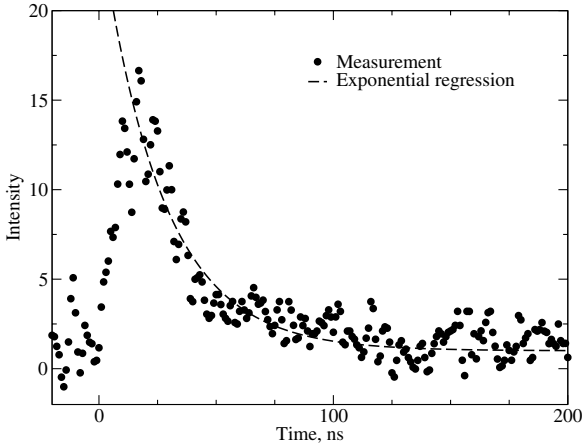

Fig. 6 Time-resolved fluorescence measurement with an exponential fit.

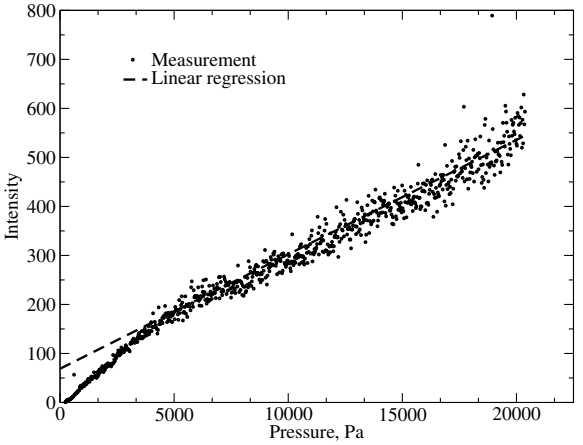

Fig. 7 Rayleigh calibration measurement in PWK3.

$$n_0 = \frac{S_V 4\pi^2 A_L (\hbar\omega_{02})^2 \sqrt{\pi}\tau_p}{D A_{21} \tau_L E_L^2 \sigma_\omega^{(2)}} \tag{5}$$

where S_V corresponds to the value of the fluorescence signal at the data acquisition system in the unit of volts at the peak of the excitation resonance.

Rayleigh scattering experiments in atmospheric air at $\lambda = 225$ nm have been performed to assure the same geometrical conditions as during the fluorescence experiments. It has been shown, during a prior measurement campaign, that the calibration using Rayleigh scattering at $\lambda = 225$ nm leads, at least within the measurement error, to the same results as measurements with Rayleigh scattering calibration at the fluorescence wavelength of $\lambda = 844$ nm [15,17]. In fact, the crucial factor for Rayleigh scattering is the absolute value of the wavelength to be used, because the Rayleigh scattering signal depends on a power of four on the wavelength [see Eq. (7)]. In the present investigation, the wavelength was measured using a wavemeter with an accuracy of 0.1 pm. The diminishing influence of the interference filter had to be added after the scattering experiment from the data sheet ($\eta = 0.42$), because the Rayleigh scattering signal would be blocked by the filter, whereas the sensitivity of the PMT is constant. The Rayleigh scattering signal for detection at 90 deg with respect to the laser beam path is

$$V_R = D\left(\frac{\mathrm{d}\sigma}{\mathrm{d}\Omega}\right)_{\mathrm{pol}}^{90\,\mathrm{deg}} n \frac{E_L}{h\nu} \tag{6}$$

where n is the number density that is calculated from pressure measurements [18]. The differential cross section is calculated from

$$\left(\frac{\mathrm{d}\sigma}{\mathrm{d}\Omega}\right)_{\mathrm{pol}}^{90\,\mathrm{deg}} = \frac{\pi^2}{n_s^2}\frac{(n_b - 1)^2}{\lambda^4} \tag{7}$$

where n_s is the number density at standard conditions ($T_n = 288,15$ K and $p_n = 1013$ hPa). The refraction index is calculated from the formulas of Penndorf [19]and Edlen [20]. The calibration constant is then derived from the slope of the measured intensity signal, dependent on the ambient pressure (as shown in Fig. 7) to $D = 4.58 \times 10^{-11}$ V · m · sr. At low pressures, the scattering signal is disturbed by background laser scattering in the chamber. At zero pressure, which is about 0.1 Pa in the vacuum chamber, no scattering has been measured. The slope change can be explained by background laser scattering that vanishes when the ambient pressure is high enough and significant Rayleigh scattering is measured [21]. Then, the expected linear dependence between number density and Rayleigh scattering is measured.

B. Calibration Using Xenon Two-Photon LIF

The second approach to quantify the relative signals is based on reference measurements using xenon noble gas. The idea is that the experimental setup is calibrated by measuring a known number density using a two-photon absorption of a rare gas with an excitation wavelength near that of atomic oxygen (see Fig. 8). Thus, the temporal, spatial, and spectral properties can be held constant for both measurements as long as the excitation is not influenced by saturation. Furthermore, because both measurements are two-photon excitation processes, the intensity distribution does not have to be determined explicitly. Equation (1) for unsaturated two-photon laser-induced fluorescence is hence applicable to both xenon and atomic oxygen. The known xenon quantity is then used to deduce the unknown atomic oxygen density. The solved equation is

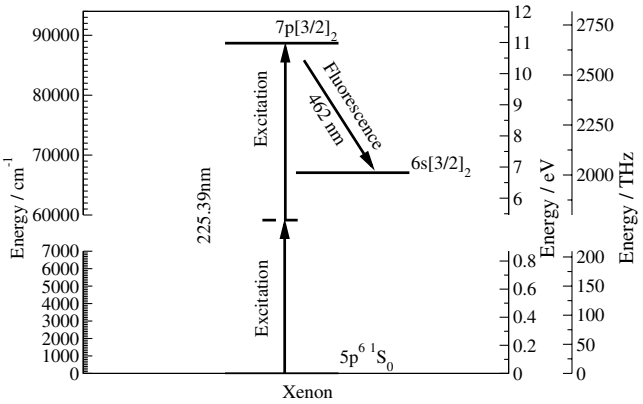

Fig. 8 Energy level diagram for xenon.

$$n_0\Big|_{\mathrm{O}} = \frac{S_{\eta,\mathrm{O}}}{S_{\eta,\mathrm{Xe}}}\frac{E_{L,\mathrm{Xe}}^2}{E_{L,\mathrm{O}}^2}\frac{\eta_{\mathrm{Xe}}}{\eta_{\mathrm{O}}} A_{21}\tau_{\mathrm{LT}}\Big|_{\mathrm{Xe}} \frac{1}{A_{21}\tau_{\mathrm{LT}}}\Big|_{\mathrm{O}} \frac{\sigma_{\omega,\mathrm{Xe}}^{(2)}}{\sigma_{\omega,\mathrm{O}}^{(2)}}\frac{g(\Delta\omega_{\mathrm{Xe}})}{g(\Delta\omega_{\mathrm{O}})} n_0\Big|_{\mathrm{Xe}} \tag{8}$$

where the indices Xe and O indicate a xenon measurement or an atomic oxygen measurement, respectively, and $g(\Delta\omega_{\mathrm{Xe}})/g(\Delta\omega_{\mathrm{O}})$ takes into account that the line widths of both measurements differ. As can be seen, all spatial and temporal influences can be reduced to one.

The two-photon LIF measurements on xenon and oxygen have been performed without changing the experimental setup at the plasma wind tunnel. To have a well-defined amount of xenon at the measurement location, a cold gas cell has been installed at the measurement location in the plasma wind tunnel PWK3. The windows of the cold gas cell are Suprasil glass windows, the diameter of which is big enough to not disturb the optical paths of the LIF measurements. Furthermore, the optical transmission of the windows is greater than 95% in the wavelength regime of interest. The cell can be evacuated down to 0.001 Pa, which is done before the cell is filled with xenon. The reference measurements were performed at a pressure of 44 Pa. The fluorescence signal as a function of the laser energy has been investigated in the same manner as described

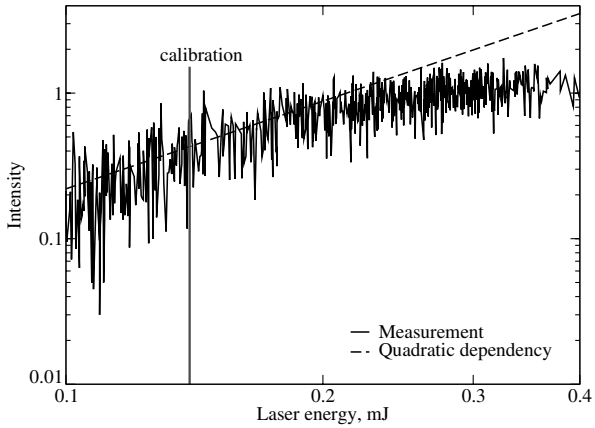

Fig. 9 Dependence of the fluorescence signal on the laser energy for xenon measurements (logarithmic scale).

previously for atomic oxygen (i.e., by turning the frequency-doubling crystal). Figure 9 shows the quadratic behavior in the energy range at which the measurements were performed ($E_L = 0.139$ mJ). The intensity variation is thereby due to the energy fluctuations of the excimer laser. Because of the low saturation level of xenon, the energy has been lowered for the calibration measurement, using a lower discharge voltage at the excimer laser. As already mentioned, this has no effect on the properties of the laser beam. Similar calibration values can be found in [11,12].

To measure the quenching influence, a pressure variation has been performed and the lifetime has been evaluated. Figure 10 shows the lifetime inversely plotted as a function of the xenon pressure. An extrapolation to zero pressure leads to the spontaneous Einstein coefficient of emission. In the present experiment, A_{21} has been measured to $A_{21} = 0.074 \times 10^8$ s^{-1}. This value corresponds well to values found in [22].

For the calibration experiment, Fig. 11 shows the fluorescence signal as a function of the absorption wavelength. From the described calibration experiment, the unknown atomic oxygen density can be measured using Eq. (8). The line width has been estimated from the full width at half maximum of each experimental data file. The two-photon cross-sectional ratio is measured using the experimentally estimated cross section of Bamford et al. [10] and measured using titration experiments [11]. The estimated value is

$$\frac{\sigma^{(2)}_{\omega,\mathrm{Xe}}}{\sigma^{(2)}_{\omega,\mathrm{O}}} = 0.36 \pm 0.18 \tag{9}$$

It should be noted that the same authors also published a cross-sectional ratio of $\sigma^{(2)}_{\omega,\mathrm{Xe}}/\sigma^{(2)}_{\omega,\mathrm{O}} = 0.51$, which is 42% higher than the value of $\sigma^{(2)}_{\omega,\mathrm{Xe}}/\sigma^{(2)}_{\omega,\mathrm{O}} = 0.36$. Thus, amelioration in accuracy has not been achievable up to now with this calibration technique. The obvious advantage of this calibration technique is the very simple applicability of xenon two-photon LIF measurements and the fewer parameters to be estimated separately. Even the cell measurement does not necessarily have to be built up if the vacuum chamber can be evacuated down to very low ambient pressures and a thoroughly measurable amount of xenon can be reached and held throughout an experiment.

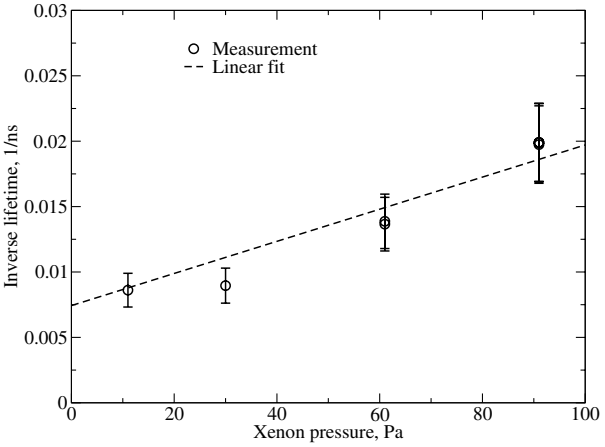

Fig. 10 Inverse lifetime of the upper xenon level derived from the duration of the fluorescence signal as a function of filling pressure.

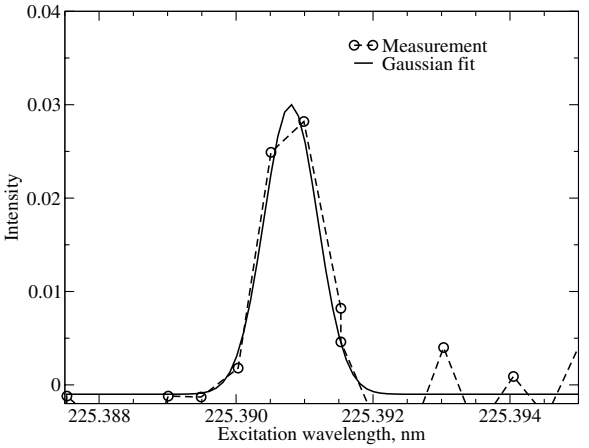

Fig. 11 Calibration experiment at $p_{\mathrm{Xe}} = 44$ Pa.

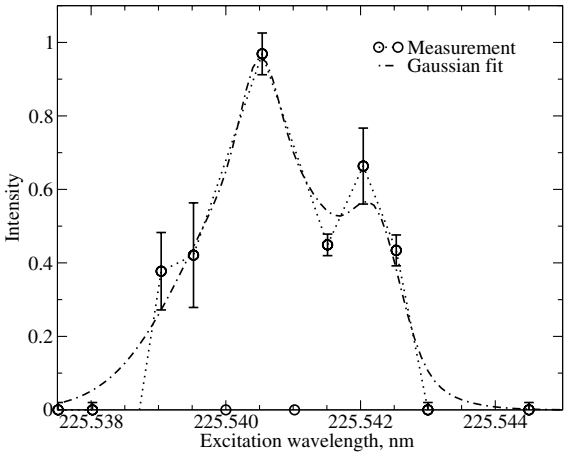

Fig. 12 LIF signal as a function of the laser wavelength ($\dot{m} = 3$ g/s, $p_A = 26$ Pa, and $U_A = 6300$ V).

IV. Results

Figure 12 shows the result of one excitation scan, that is, the fluorescence intensity as a function of the excitation wavelength. Each LIF experiment has been performed as a so-called wavelength scan. At steady-state plasma generator conditions, which are usually indicated by a constant electrical power consumption and constant cooling water temperatures, ten laser pulses at each wavelength step along the absorption line profile are recorded. The minimum step size of the laser system is 0.001 nm. Furthermore, Fig. 12 shows a fit using three Gaussian curves from which temperatures and densities are estimated. In this paper, emphasis lies on the number density. Two values along the scan were disturbed by the high frequency of the plasma generator and are not taken into account for evaluation. However, this effect occurred only at the very-high-power conditions ($U_A \geq 6000$ V) of the generator. Nevertheless, the absorption profile can clearly be identified. The indicated error bars are determined from the standard deviation of the ten laser pulses. The effective lifetime is evaluated from the simultaneously recorded

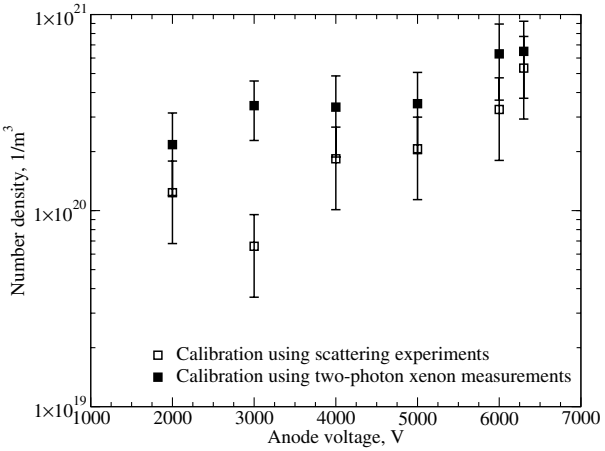

Fig. 13 Experimentally estimated number densities of atomic oxygen using both calibration techniques as a function of the anode voltage of the generator ($\dot{m} = 3$ g/s and $p_A = 26$ Pa); filled symbols indicate calibration using a xenon reference measurement).

time-resolved fluorescence signal. Together with the presented calibration techniques, the number densities can be determined.

In Fig. 13, the measured number densities that depend on the anode voltage of the plasma generator are plotted for both calibration approaches. The inflow of oxygen into the generator is held constant at $\dot{m} = 3$ g/s. In general, increasing input power leads to higher dissociation and thus to higher atomic oxygen number densities. The maximum number density reached is of the order of 1×10^{21} $1/\mathrm{m}^3$. According to calculations of Huang and Gordon [23], amplified spontaneous emission (ASE) could influence the deexcitation. However, the measurements that vary the laser energy should show this effect by a beginning nonlinearity (see Fig. 5), but, obviously, the ASE threshold is not yet reached.

At lower anode voltage, the facility is in a capacitive discharge mode and switches to the inductive heating mode with a discrete step at about $U_A = 3000$ to 4500 V [5]. In the inductive mode, the coupling efficiency is higher than in the capacitive discharge mode, which is seen from the fact that the cooling water losses in the inductive mode are lower (i.e., more input power results in plasma flow enthalpy). At an anode voltage of 6300 V, the translational temperature is about 3500 K and almost full dissociation is reached. The local mass-specific enthalpy is about 30 MJ/kg [15]. Both calibration techniques lead, within the measurement accuracy, to the same result. The exceptionally high deviation at the anode voltage of 3000 V can be explained by the facility behavior. As mentioned, between 3000 and 4500 V, the plasma state switches from a discharge mode with lower coupling efficiency to an inductive high-enthalpy mode [5]. In this operation regime, the reproducibility of the plasma state is weak. The data plotted here at 3000 V are right below the switch.

Going into more detail, it can be seen that there is an almost constant discrepancy between the two results. This indicates that there is a systematic error in the measurements. However, the only uncertainty in the measurement using the xenon reference measurement is the cross-sectional ratio, as discussed previously. For example, a cross-sectional ratio of 0.2, which is still within the accuracy range, results in the same number densities [11]. On the other hand, the calibration using scattering experiments has more possibilities for systematic errors. A direct influence is, for example, the measurement of the laser beam area at the measurement location. This has been measured using variable diaphragms leading to an accuracy of only 50%. Here, the same conclusion can be made: modifying the laser beam area within half of the measurement accuracy brings the results in very good agreement. The main drawback of the scattering experiment is, however, that from a quantum mechanical point of view, a different process is used to simulate a light signal at the measurement location in order to calibrate the sensitivity of the measurement equipment. Although it is assumed that the same behavior occurs afterward in two-photon LIF (i.e., the same spatial behavior of Rayleigh scattering and fluorescence emission is assumed), there is no possibility to check whether the assumption is correct. Consequently, the constant discrepancy between the two calibration methods can also simply result from the fact that the calibration technique using scattering experiments leads to lower number density, due to the quantum physical reason that, in contrast to the LIF process, no energy exchange occurs during the Rayleigh scattering process as an elastic scattering process. From an experimental point of view, the new approach using reference measurements on xenon is much simpler and has fewer input parameters that have to be measured in order to determine number densities.

V. Conclusions

Laser-induced fluorescence measurements have been performed at the inductively heated plasma wind tunnel PWK3 in pure oxygen plasma flows using two calibration methods. The relative measurements were first calibrated using standard scattering experiments, such that the sensitivity of the data acquisition setup was measured using a second measurement. Although Raman scattering measurement is usually applied, in the present case, Rayleigh scattering has been applied, because the Raman signal is too weak for this application. As a second calibration method, reference measurements on xenon have been performed. Because the excitation wavelength of xenon and atomic oxygen is almost the same, only the cross-sectional ratio and the fluorescence wavelength has to be considered.

The measurements show that both calibration techniques lead to the same result within the measurement accuracy. However, the constant discrepancy leads to the assumption that there is a systematic measurement error. Although the calibration using scattering experiments has many factors to be measured separately, the only variable using the xenon reference measurement is the cross-sectional ratio. Assuming a cross-sectional ratio of 0.2, which is still within the accuracy of the ratio given in literature, very good agreement of the measurements is achieved. Because of the very high sensitivity of the LIF measurement technique, which is actually one of its advantages, a further step has to be the amelioration of the accuracy of the cross-sectional ratio.

For an amelioration of the measurement, it is necessary to lower the uncertainty in the cross-sectional ratio. Therefore, measurements at PWK3 , together with correlation measurements, are foreseen at very low anode voltages using the probe technique. Meanwhile, solid electrolyte sensors that are fairly sensitive for atomic oxygen are also available at the institute. At low-enthalpy conditions, these sensors can be used in the plasma wind tunnel. It is supposed that calibration measurements using these sensors and the xenon calibration procedure can be used to lower the uncertainty in the cross-sectional ratio.

Acknowledgments

The authors gratefully acknowledge the funding of this work through the Deutsche Forschungsgemeinschaft (DFG) project Au85/24-1. The authors also wish to acknowledge the help of G. Herdrich and H. Böhrk.

References

[1] Lu, F., and Marren, D. (eds.), *Advanced Hypersonic Test Facilities*, Vol. 198, Progress in Astronautics and Aeronautics, AIAA, Reston, VA, 2002.

[2] Herdrich, G., Löhle, S., Pidan, S., Auweter-Kurtz, M., and Laux, T., "IRS Ground-Testing Facilities: Thermal Protection System Development, Code Validation and Flight Experiment Development," *Journal of Spacecraft and Rockets*, Vol. 42, No. 5, 2005, pp. 817–824.

[3] Fasoulas, S., "Experimentelle und theoretische Charakterisierung Einer Hochenthalpen Stickstoffströmung zur Wiedereintrittssimulation," Ph. D. Thesis, Institut für Raumfahrsysteme, Univ. of Stuttgart, Stuttgart, Germany, 1995.

[4] Herdrich, G., Auweter-Kurtz, M., Endlich, P., and Kurtz, H., "Mars

Entry Simulation Using an Inductively Heated Plasma Generator," *Journal of Spacecraft and Rockets*, Vol. 40, No. 5, 2003, pp. 690–694.

[5] Herdrich, G., Auweter-Kurtz, M., Laux, T., and Winter, M., "Operational Behaviour of Inductively Heated Plasma Source IPG3 for Entry Simulations," *Journal of Thermophysics and Heat Transfer*, Vol. 16, No. 3, 2002, pp. 440–449.

[6] Herdrich, G., Löhle, S., Auweter-Kurtz, M., Endlich, P., Fertig, M., Pidan, S., and Schreiber, E., "IRS Ground-Testing Facilities: Thermal Protection System Development, Code Validation and Flight Experiment Development," AIAA Paper 2004-2596, 2004.

[7] Löhle, S., Auweter-Kurtz, M., Pidan, S., and Herdrich, G., "Laser-Induced Fluorescence Measurements in Inductively Heated High-Enthalpy Plasma Flows," AIAA Paper 2005-5324, 2005.

[8] Döbele, H.-F., Czarnetzki, U., and Goehlich, A., "Diagnostics of Atoms by Laser Spectroscopic Methods in Plasmas and Plasma-Wall Interaction Studies (Vacuum Ultraviolet and Two-Photon Techniques)," *Plasma Sources Science and Technology* , Vol. 9, Sept. 2000, pp. 477–491.

[9] Döbele, H.-F., Mosbach, T., Niemi, K., and von der Gathen, V. S., "Laser-Induced Fluorescence Measurements of Absolute Atomic Densities: Concepts and Limitations," *Plasma Sources Science and Technology* , Vol. 14, May 2005, pp. S31–S41.

[10] Bamford, D., Jusinski, L., and Bischel, W., "Absolute Two-Photon Absorption and Three-Photon Ionization Cross Sections for Atomic Oxygen," *Physical Review A*, Vol. 34, No. 1, 1986, pp. 185–198.

[11] Niemi, K., von der Gathen, V. S., and Döbele, H.-F., "Absolute Calibration of Atomic Density Measurements by Laser-Induced Fluorescence Spectroscopy with Two-Photon Excitation," *Journal of Physics D: Applied Physics*, Vol. 34, July 2001, pp. 2330–2335.

[12] Goehlich, A., Kawetzki, T., and Döbele, H.-F., "On Absolute Calibration with Xenon of Laser Diagnostic Methods Based on Two-Photon Absorption," *Journal of Chemical Physics*, Vol. 108, No. 22, 1998, pp. 9362–9370.

[13] Grinstead, J., Driver, D. M., and Raiche, G. A., "Optical Diagnostics Development for the Ames Arcjet Facilities," AIAA Paper 2002-398, 2002.

[14] Herdrich, G., Auweter-Kurtz, M., Endlich, P., Kurtz, H., Laux, T., Löhle, S., Nazina, N., Pidan, S., Schreiber, E., Wegmann, T., and Winter, M., "Atmospheric Entry Simulation Capabilities at IRS," *3rd International Symposium on Atmospheric Reentry Vehicles and Systems* [CD ROM], Association Aéronautique et Astronautique de France, Paris, France, 2003.

[15] Löhle, S., "Untersuchung von Wiedereintrittsplasmen mit Hilfe laserinduzierter Fluoreszenzmessungen," Ph.D. Thesis, Institut für Raumfahrsysteme, Univ. of Stuttgart, Stuttgart, Germany, 2006.

[16] Wiese, W., Smith, M., and Glennon, B., *Atomic Transition Probabilities: Hydrogen Through Neon*, National Bureau of Standards, Gaithersburg, MD, 1966.

[17] Feigl, M., Dennis, J., Fasoulas, S., and Auweter-Kurtz, M., "Comparison of LIF and Solid Electrolyte Sensor Measurements of Atomic and Molecular Oxygen in a Plasma Jet," AIAA Paper 2000-0198, 2000.

[18] Eckbreth, A., *Laser Diagnostics for Combustion Temperature and Species*, 2nd ed., Energy and Engineering Science Series, Abacus Press, Cambridge, MA, 1988..

[19] Penndorf, R., "Tables of Refractive Index for Standard Air and the Rayleigh Scattering Coefficient for the Spectral Range Between 0.2 and 20.0μ and Their Application to Atmospheric Optics," *Journal of the Optical Society of America*, Vol. 47, No. 2, 1957, pp. 176–182.

[20] Edlen, B., "The Refractive Index of Air," *Metrologia*, Vol. 2, No. 2, 1966, pp. 71–80.

[21] Hirsch, K., "Streudiagnostik mit Stationären Argonionenlasern am Magnetfeldstabilisierten Bogen," Ph.D. Thesis, Institut für Plasmaforschung, Univ. of Stuttgart, Stuttgart, Germany, 1975.

[22] Horiguchi, H., Chang, R., and Setser, D., "Radiative Lifetimes and Two-Body Collisional Deactivation Rate Constants in Ar for Xe(5p 56p), Xe(5p 56p), and Xe(5p 57p) States," *Journal of Chemical Physics*, Vol. 75, No. 3, 1981.

[23] Huang, Y.-L., and Gordon, R., "The Effect of Amplified Spontaneous Emission on the Measurement of the Multiplet State Distribution of Ground State Oxygen Atoms," *Journal of Chemical Physics*, Vol. 97, No. 9, 1992.